Resolution of Structural Changes Associated with Calcium Activation of Calmodulin Using Frequency Domain Fluorescence Spectroscopy†

Yihong Yao,‡ Christian Schöneich,§ and Thomas C. Squier*,‡

Departments of Biochemistry and Pharmaceutical Chemistry, University of Kansas, Lawrence, Kansas 66045-2106

Received January 6, 1994; Revised Manuscript Received April 11, 1994®

ABSTRACT: Structural changes associated with the calcium-dependent activation of wheat germ calmodulin (CaM) were assessed through measurements of steady-state and time-resolved changes in the fluorescence associated with (1) the unique tyrosine (Tyr_{139}) located in calcium binding loop IV or (2) *N*-(1-pyrenyl)-maleimide (PM) or 4-(iodoacetamido)salicylic acid (IASA) covalently attached to Cys_{27} present in calcium binding loop I. These fluorophores permit the measurement of calcium-dependent changes in (i) the solvent accessibility and rotational dynamics associated with calcium binding loops I and IV and (ii) the hydrodynamic properties of the entire protein. Specific nitration of the unique tyrosine (Tyr_{139}) in calcium binding loop IV permits the use of fluorescence resonance energy transfer to measure both the average spatial separation and distance heterogeneity between Cys_{27} and Tyr_{139}, providing a direct measurement of the conformational flexibility of the central helix. Upon calcium binding, (i) the solvent accessibility and rotational dynamics of both PM and IASA (covalently bound to Cys_{27}) and Tyr_{139} increase, (ii) overall protein rotational motion decreases, (iii) the average separation between the chromophores at Cys_{27} and nitrotyrosine 139 decreases, and (iv) the conformational flexibility associated with the central helix decreases. Therefore, upon calcium binding, the central helix becomes more extended and rigid, while the globular domains adopt a more open tertiary conformation that brings Cys_{27} and Tyr_{139} into closer proximity. This calcium-dependent structural change functions to expose the hydrophobic binding sites located within the globular domains, and to enhance the probability of binding target sequences through a reduction in conformational heterogeneity.

Calmodulin (CaM)[1] is a ubiquitous eukaryotic Ca^{2+}-binding protein that regulates numerous cellular processes, including muscle contraction, neurotransmission, neuronal plasticity, cytoskeletal assembly, and a host of reactions involved in the energy and biosynthetic metabolism of the cell [reviewed by Wylie and Vanaman (1988)]. The crystal structure of the calcium-liganded form of CaM has recently been refined to 1.7 Å (Chattopadhyaya et al., 1992) and shows two structurally homologous, globular domains connected by an eight-turn central α-helix (Babu et al., 1985, 1988). Both globular domains consist of two Ca^{2+}-binding sites, each of which shows a helix–loop–helix motif known as an EF-hand (Kretsinger & Nockolds, 1973). Binding of Ca^{2+} is cooperative with respect to each globular domain, and this binding functions to induce a conformational change that is thought to expose an otherwise inaccessible nonpolar surface involved in target enzyme binding, which leads to the activation of various target enzymes (Tanaka & Hidaka, 1980). Calcium binding sites II and III are associated with the central helix, suggesting that structural changes involving the central helix may play a critical role in the cooperative binding of calcium (Babu et al., 1985). However, while there is evidence that the two opposing domains of CaM do interact [Johnson, 1983; Yoshida et al., 1983; Thulin, et al., 1984; reviewed by Klee (1988)], a cooperative enhancement in calcium binding between these two domains has only been observed in the presence of target peptides (Yazawa et al., 1992), which involves the association of both opposing globular domains in CaM (Meador et al., 1992; Ikura et al., 1992b; Meador et al., 1993). Therefore, it remains unclear whether structural changes associated with the central helix play any role in the calcium-dependent activation of CaM.

X-ray structural data is available only for the calcium-liganded form of CaM at acidic pH (i.e., pH 5.0 and 5.6) in the presence of helicogenic solvents (i.e., nonaqueous solvents that appear to induce additional α-helix; Bayley et al., 1988). Therefore, it remains unclear as to the nature of both (i) the structural changes associated with calcium activation and (ii) the average structure of CaM in solution under physiological conditions. In fact, significant differences have been observed in both the secondary and tertiary structures of CaM as a function of both pH and salt concentration (Török et al., 1992). Hydrodynamic measurements using both optical and magnetic resonance techniques suggest that CaM is more compact at physiological pH relative to acidic conditions analogous to those used to obtain the crystal structure (Wang, 1989; Small & Anderson, 1988; Heidorn & Trewhella, 1988; Török et al., 1992). Likewise, it has been suggested that CaM becomes

† Supported in part by grants from the National Institutes of Health (GM46837), the Muscular Dystrophy Association, and the University of Kansas.

* Correspondence should be addressed to Dr. Thomas C. Squier (913-864-4081).

‡ Department of Biochemistry.

§ Department of Pharmaceutical Chemistry.

® Abstract published in *Advance ACS Abstracts,* June 1, 1994.

[1] Abbreviations: IAEDANS, 5-[[2-[(iodoacetyl)amino]ethyl]amino]-naphthalene-1-sulfonic acid; CaM, calmodulin; DTNB, 5,5′-dithiobis-(2-nitrobenzoic acid); DTT, dithiothreitol; EDTA, ethylenediaminetetraacetic acid; FRET, fluorescence resonance energy transfer; FURA-2, 1-[[2-(5-carboxyoxazol-2-yl)-6-aminobenzofuran-5-yl]oxy]-2-(2′-amino-5′-methylphenoxy)ethane-*N*,*N*,*N*′,*N*′-tetraacetic acid; HEPES, *N*-(2-hydroxyethyl)piperazine-*N*′-2-ethanesulfonic acid; GnHCl, guanidinium hydrochloride; HOMOPIPES, homopiperazine-*N*,*N*′-bis(2-ethanesulfonic acid); HPLC, high-performance liquid chromatography; IASA, 4-(iodoacetamido)salicylic acid; PM, *N*-(1-pyrenyl)maleimide; SDS, sodium dodecyl sulfate; TEMPAMINE, 4-amino-2,2,6,6-tetramethyl-1-piperidinyloxyl; TFA, trifluoroacetic acid; TNM, tetranitromethane.

0006-2960/94/0433-7797$04.50/0

extended upon calcium binding at physiological pH [LaPorte et al., 1981; Seaton et al., 1985; Small & Anderson, 1988; Heidorn & Trewhella, 1988; reviewed by Trewhella (1992)], although possible structural linkages between the two globular domains (in the absence of target peptides) remain controversial [Barbato et al., 1992; Török et al., 1992; reviewed by Williams (1992); reviewed by Kretsinger (1992a)]. Subsequent to calcium activation, the critical element associated with binding target enzymes appears to involve the flexibility of the central helix, as the association of the calcium-activated form of CaM with target peptides results in only minimal changes in the conformation of the opposing globular domains (Meador et al., 1992; Ikura et al., 1992b; Meador et al., 1993). Therefore, central to the question of how calcium activation of CaM facilitates its specific interaction with target sequences is information regarding the structure of the globular domains as well as that of the central helix. In this regard, fluorescence spectroscopy is a sensitive tool for studying the structure and dynamics of proteins [reviewed by Lakowicz and Gryczynski (1991)]. Using fluorescence anisotropy and quenching experiments we are able to specifically probe both the global conformation of CaM (i.e., hydrodynamic properties) and the localized structure associated with the globular domains. In addition, through the use of fluorescence resonance energy transfer (FRET) we are able to measure the conformational heterogeneity associated with the central linker helix that connects the two opposing globular domains [reviewed by Cheung (1991)].

This study takes advantage of the single cysteine and tyrosine present in wheat germ CaM, which can be modified to provide fluorescence signals used to assess the calcium-dependent structural changes of CaM. Wheat germ CaM has 94% sequence identity with bovine brain CaM (Klee et al., 1980; Toda et al., 1985) and previously has been shown to fully activate a range of target proteins from human and animal sources (Strasburg et al., 1988). Our measurements involve the specific labeling of the unique cysteine group (Cys_{27}) available in wheat germ CaM with two different sulfhydryl group directed chromophores, which serve as energy-transfer donors. Likewise, we are able to use the intrinsic fluorescence associated with the single tyrosine (Tyr_{139}) in the carboxyl domain to assess structural changes associated with calcium binding. Alternatively, the selective nitration of this tyrosine with tetranitromethane (TNM) permits its use as an energy-transfer acceptor, permitting direct measurements of the spatial separation between the globular domains of CaM. This latter measurement provides direct information relating to both the average structure and conformational heterogeneity of the central helix. Together, these complementary measurements of both the local and global conformation and dynamics associated with calcium activation permit us to distinguish between alternative models relating to the structural changes in both the globular domains and central helix associated with calcium binding to CaM.

EXPERIMENTAL PROCEDURES

Materials. IASA [4-(iodoacetamido)salicylic acid] and PM [*N*-(1-pyrenyl)maleimide] were obtained from Molecular Probes, Inc. (Junction City, OR). TEMPAMINE (4-amino-2,2,6,6-tetramethyl-1-piperidinyloxyl) and TNM (tetranitromethane) were obtained from Aldrich (Milwaukee, WI). Immediately prior to its use, TNM was purified by extracting four times with a 20-fold excess volume of water (Riordan & Vallee, 1972). Purified FURA-2 was generously provided by Professor J. David Johnson (Ohio State University). All other chemicals were of the purest grade commercially available.

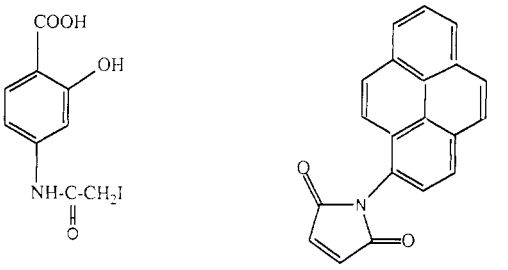

4-Iodoacetamidosalicylic acid Pyrene-Maleimide

FIGURE 1: Chemical structures: (a) 4-(iodoacetamido)salicylic acid (IASA) and (b) *N*-(1-pyrenyl)maleimide (PM).

CaM was purified from wheat germ using the procedure outlined by Strasburg et al. (1988). Purity was assessed using both SDS–PAGE, where CaM migrates as a single band, and HPLC. Purified wheat germ CaM was stored at −70 °C. Human erythrocyte ghosts were prepared essentially as described by Niggli et al. (1979).

Specific Derivatization of Cys_{27}. Prior to chemical derivatization, CaM is first dissolved in 6 M GnHCl, 25 mM HEPES (pH 7.5), 50 mM DTT, and 1 mM EDTA and incubated at 25 °C for 2 h in order to eliminate intermolecular cross-linking. DTT was removed by dialysis of the protein against deionized water prior to lyophilization. Sulfhydryl content was measured by the method described by Ellman (1959). Specificity of labeling was assured by (i) titration of remaining sulfhydryl groups using DTNB (ϵ_{412} = 13 600 M^{-1} cm^{-1}), (ii) quantitation of bound fluorophore using the molar extinction coefficient (see below), and (iii) identification of labeled peptide(s) subsequent to proteolytic digestion using HPLC (see below).

Chemical derivatization of Cys_{27} with pyrenylmaleimide (PM) (Figure 1) was carried out in the dark. The concentration of PM was kept below 20 μM to avoid nonspecific probe aggregation. Briefly, 12 μM PM was added to a solution containing 6 μM CaM (i.e., 0.1 mg/mL) in 0.1 mM $CaCl_2$, 25 mM HEPES (pH 7.5) at 25 °C. The reaction was quenched after 1 h by the addition of 0.1 mM DTT to the reaction mixture, which was incubated on ice for 10 min. The labeled CaM was separated from unreacted PM using a Sephadex G-25 column (1.6 × 23 cm) and was subsequently lyophilized. The specific labeling of Cys_{27} with 4-(iodoacetamido)salicylic acid (IASA) was essentially identical to that of PM, except that a 10-fold molar excess of IASA was added to CaM in the presence of 6 M GnHCl, essentially as described by Strasburg et al. (1988) for the labeling of CaM with IAEDANS. Incorporation of IASA and PM was determined using their molar extinction coefficients, ϵ_{302} = 9500 M^{-1} cm^{-1} and ϵ_{343} = 36 000 M^{-1} cm^{-1} for IASA and PM, respectively (Haugland, 1992). Protein concentration was routinely determined using the micro BCA assay (Pierce). A stock solution of CaM, whose concentration was determined using the published extinction coefficient for CaM (Strasburg et al., 1988), was used as a protein standard.

Selective Nitration of Tyr_{139}. Nitration with freshly purified TNM was carried out at 25 °C in the presence of 60 μM CaM (i.e., 1.0 mg/mL) in 1 M NaCl, 0.5 mM $CaCl_2$, and 0.1 M TRIS (pH 7.9), essentially as previously described (Richman & Klee, 1978). The nitration of Tyr_{139} was initiated by the addition of saturating concentrations of TNM in ethanol (i.e., 15%, v/v) to give a final concentration of 100-fold molar excess TNM relative to CaM. Subsequent to the addition of TNM,

the aqueous phase was immediately separated from the nonsoluble oil. After 1 h the reaction was quenched by adding excess β-mercaptoethanol and left on ice for 10 min prior to the separation of the derivatized CaM using a Sepharose G-25 column (1.6 × 23 cm). Derivatized CaM was stable at −70 °C for 2 months, as evidenced by both the ability to activate the erythrocyte Ca-ATPase and fluorescence measurements relating to protein structural changes (see Results). The extent of nitration was measured in 6 M GnHCl, 1 mM EDTA, and 25 mM HEPES (pH 10) using the molar extinction coefficient ϵ_{428} = 4200 M^{-1} cm^{-1} for nitrotyrosine (Richman & Klee, 1978).

Enzymatic Assays. The Ca-ATPase activity of erythrocyte ghosts was determined using the methods described by Lanzetta et al. (1979), essentially as described previously for sarcoplasmic reticulum Ca-ATPase (Squier & Thomas, 1988). When applicable, the free calcium concentration was calculated using a modified version of the computer program previously described (Fabiato & Fabiato, 1979; Fabiato, 1988), which calculates the multiple equilibria between all ligands in solution. The free calcium concentration was checked using the calcium indicator dye FURA-2 (λ_{ex} = 340 nm; λ_{em} = 510 nm). In all cases we find an apparent dissociation constant of ≈80 ± 5 nM, in close agreement with literature values [K_D ≈ 0.1 mM; Haugland (1992)].

Identification of Tryptic Fragments. In order to access sites associated with chemical derivatization, calmodulin (60 μM) was subjected to exhaustive tryptic digestion (0.6 μM trypsin in 50 mM potassium phosphate at pH 8.0 for 9 h at 37 °C). Digestion was stopped upon the addition of 1.8 μM trypsin inhibitor. Tryptic fragments were separated on HPLC using a Vydac C4 reverse phase column employing a linear gradient varying from 0.1% trifluoroacetic acid (TFA) to 0.1% TFA in 80% acetonitrile/20% water at a rate of 1%/min. The respective peaks were monitored at 214 nm. The detected peaks were pooled, lyophilized, and subjected to FAB mass spectrometry. Details relating to the assignments of these peaks will be published elsewhere.

Spectroscopic Measurements. Fluorescence emission spectra were recorded using an ISS K2 fluorometer in the ratio mode. Excitation was set at 302 nm for IASA-labeled CaM and 351 nm for PM-labeled CaM. Emission slits were adjusted to a 4-nm bandwidth, and the sample temperature was maintained at 25 °C. Fluorescence lifetime and anisotropy measurements were performed using an ISS K2 frequency domain fluorometer, whose design has previously been described in detail (Gratton & Limkeman, 1983). This instrument is equipped with a Marconi signal generator (2022A & C) and ENI broad-band amplifiers (325LA and 403LA) which operate in conjunction with a Pockels cell to obtain intensity-modulated light from either a 300-W xenon arc lamp (ILC Technology PS300-1) or alternatively a CW argon ion laser equipped with extended UV capabilities (Coherent Innova 400/2/0.3, Santa Clara, CA).

Fluorescence quenching experiments were performed using an ISS K2 fluorometer in the ratio mode. TEMPAMINE was added in microliter increments to 2 mL of either 1.1 μM PM- or IASA-labeled CaM dissolved in 0.1 M KCl, 25 mM HEPES (pH 7.5), and either 0.1 mM $CaCl_2$ or 0.1 mM EDTA. Excitation was at 351 and 302 nm, respectively. Fluorescence emission was collected using a Schott GG400 long-pass filter. Alternatively, analogous experiments involving tyrosine quenching used 5.9 μM native CaM, with 275-nm excitation. In the latter case fluorescence emission was collected through an Oriel band-pass filter centered at 320 nm (full width half-maximum is 10 nm), and necessary corrections were made for the contribution to the observed fluorescence intensity originating from Raman scattering. For comparison purposes, KI (1 M stock) was also used as a collisional quencher. Analysis of the collisional quenching was carried out essentially as described by Lehrer and Leavis (1978) and is described in the footnotes below Table 2.

Decays of Fluorescence Intensity. The time-dependent decay $I(t)$ of any fluorophore can always be described as a sum of exponentials,

$$I(t) = \sum_{i=1}^{n} \alpha_i e^{-t/\tau_i} \quad (1)$$

where α_i are the preexponential factors, τ_i are the excited-state decay times, and n is the number of exponential components required to describe the decay. The intensity decay law is obtained from the frequency response of the amplitude-modulated light and is characterized by the frequency-dependent values of the phase shift and the extent of demodulation, whose respective errors are assumed to be 0.2° and 0.005. The parameters describing the decay law are compared with the calculated values from an assumed decay law, and the parameters chosen are those that minimize the squared deviation. Explicit expressions have been provided that permit the ready calculation of α_i and τ_i (Weber, 1981). The parameter values are determined by minimizing the χ_R^2 (the F statistic), which serves as a goodness-of-fit parameter that provides a quantitative comparison of the adequacy of different assumed models (Lakowicz & Gryczynski, 1991). Data are fitted using the method of nonlinear least squares to a sum of exponential decays (Bevington, 1969). Subsequent to the measurement of the intensity decay, one typically calculates the average lifetime, $\bar{\tau}$, which is weighted by the amplitudes associated with each of the preexponential terms, where

$$\bar{\tau} \equiv \sum_i \alpha_i \tau_i \quad (2)$$

$\bar{\tau}$ is directly related to the average time the fluorophore is in the excited state, and the amplitude weighting implies a direct relationship between $\bar{\tau}$ and the quantum yield of the fluorophore (Luedtke et al., 1981). Alternatively, for the case of resonance energy transfer measurements more realistic physical models were used involving a distribution of distances (see below), as previously described (Lakowicz et al., 1988).

Calculation of Molecular Distances Using FRET. Utilizing fluorescence resonance energy transfer (FRET) to measure the distance between any fluorophore (donor; D) and a suitable acceptor (A) chromophore, one can measure distances in the 10–100-Å range and directly recover structural information concerning biological macromolecules (Stryer, 1978). The efficiency of energy transfer, E, and the apparent donor–acceptor distance, r_{app}, are calculated from the Förster equations (Fairclough & Cantor, 1978), where

$$E = 1 - \frac{F_{da}}{F_d} = 1 - \frac{\bar{\tau}_{da}}{\bar{\tau}_d} \quad \text{and} \quad E = \frac{R_0^6}{R_0^6 + r_{app}^6} \quad (3)$$

F_{da} and F_d are the steady-state fluorescence intensities in the presence and absence of the acceptor (nitrotyrosine), $\bar{\tau}_{da}$ and $\bar{\tau}_d$ are the average fluorescence lifetimes (see eq 2) of the donor in the presence and absence of the acceptor (nitrotyrosine), and R_0 is the Förster critical distance that defines the distance for a given donor–acceptor pair where the efficiency of resonance energy transfer is 50%. $\bar{\tau}_{da}$ and $\bar{\tau}_d$ are determined from frequency domain measurements relating to the fluo-

Table 1

A. Lifetime Data for PM-CaM in the Presence and Absence of Nitrotyrosine[a]

sample	pH	α_1	τ_1 (ns)	α_2	τ_2 (ns)	α_3	τ_3 (ns)	$\sum\alpha_i\tau_i$ (ns)	$\chi_R^{2\,b}$
D + Ca^{2+}	7.5	0.788	3.72	0.136	18.8	0.076	115.4	13.5	1.8
		(0.031)	(0.04)	(0.008)	(0.6)	(0.004)	(3.2)	(0.2)	(10.8)
DA + Ca^{2+}	7.5	0.808	3.45	0.141	18.1	0.031	107.2	8.66	2.2
		(0.025)	(0.03)	(0.011)	(0.4)	(0.001)	(2.3)	(0.1)	(34.7)
D – Ca^{2+}	7.5	0.611	3.45	0.251	14.8	0.138	96.9	19.2	1.1
		(0.021)	(0.02)	(0.009)	(0.3)	(0.003)	(2.2)	(0.1)	(16.9)
DA – Ca^{2+}	7.5	0.552	2.66	0.352	11.9	0.096	92.8	14.6	1.8
		(0.17)	(0.17)	(0.011)	(0.3)	(0.002)	(2.9)	(0.2)	(27.2)
D + Ca^{2+}	5.0	0.632	3.43	0.279	20.5	0.089	125.4	19.2	1.4
		(0.02)	(0.08)	(0.012)	(0.5)	(0.004)	(4.3)	(0.3)	(12.2)
DA + Ca^{2+}	5.0	0.727	3.34	0.200	18.8	0.073	125.0	15.3	1.3
		(0.03)	(0.12)	(0.013)	(0.8)	(0.06)	(7.3)	(0.3)	(25.4)
D + Ca^{2+} in	7.5	0.474	1.36	0.507	4.71	0.019	42.7	3.84	0.5
6 M GnHCl		(0.008)	(0.06)	(0.009)	(0.18)	(0.001)	(0.7)	(0.06)	(8.8)
DA + Ca^{2+} in	7.5	0.544	1.27	0.438	4.69	0.018	36.8	3.40	0.6
6 M GnHCl		(0.010)	(0.07)	(0.009)	(0.17)	(0.001)	(0.6)	(0.04)	(10.2)

B. Lifetime Data for IASA-CaM in the Presence and Absence of Nitrotyrosine[c]

sample	pH	α_1	τ_1 (ns)	α_2	τ_2 (ns)	$\sum\alpha_i\tau_i$ (ns)	$\chi_R^{2\,d}$
D + Ca^{2+}	7.5	0.930	0.481	0.070	4.51	0.704	0.9
		(0.001)	(0.006)	(0.001)	(0.06)	(0.008)	(269)
DA + Ca^{2+}	7.5	0.951	0.332	0.049	3.23	0.474	1.1
		(0.003)	(0.009)	(0.002)	(0.10)	(0.007)	(128)
D – Ca^{2+}	7.5	0.915	0.430	0.086	3.88	0.727	1.6
		(0.001)	(0.006)	(0.001)	(0.06)	(0.009)	(269)
DA – Ca^{2+}	7.5	0.920	0.418	0.080	2.97	0.622	1.0
		(0.003)	(0.006)	(0.003)	(0.05)	(0.010)	(134)
D + Ca^{2+}	5.0	0.897	0.431	0.103	4.87	0.888	1.0
		(0.003)	(0.009)	(0.002)	(0.09)	(0.009)	(278)
DA + Ca^{2+}	5.0	0.944	0.408	0.056	6.04	0.727	1.7
		(0.003)	(0.012)	(0.002)	(0.15)	(0.011)	(159)

C. Lifetime Data for Tyr_{139}-CaM[e]

sample	pH	α_1	τ_1 (ns)	α_2	τ_2 (ns)	$\sum\alpha_i\tau_i$ (ns)	$\chi_R^{2\,f}$
+Ca^{2+}	7.5	0.90	0.30	0.10	2.4	0.51	1.6
		(0.01)	(0.05)	(0.01)	(0.2)	(0.06)	(95)
+EGTA	7.5	0.86	0.60	0.14	2.6	0.88	0.74
		(0.02)	(0.04)	(0.02)	(0.2)	(0.06)	(43)
+Ca^{2+}	5.0	0.85	0.30	0.15	2.4	0.62	2.0
		(0.01)	(0.06)	(0.01)	(0.2)	(0.08)	(117)

[a] Average amplitudes (α_i) and lifetimes (τ_i), obtained from three-exponential fits to frequency domain data collected for donor only (D or PM-CaM) and donor–acceptor (DA or PM-nitrotyrosine-CaM) calmodulin, represent the average of six different measurements, where uncertainties in the measured lifetime parameters (shown in parentheses) represent the standard error of the mean. [b] The χ_R^2 for a two-exponential fit to the data is shown in parentheses for comparison purposes. Experimental conditions: 25 mM HEPES (or 25 mM HOMOPIPES at pH 5.0), 0.1 M KCl, and either 0.1 mM $CaCl_2$ (+Ca^{2+}) or 0.1 mM EDTA (–Ca^{2+}) at 25 °C. [c] Average amplitudes (α_i) and lifetimes (τ_i), obtained from two-exponential fits to frequency domain data collected for donor only (D or IASA-CaM) and donor–acceptor (DA or IASA-nitrotyrosine-CaM) calmodulin, represent the average of five different measurements, where uncertainties in the measured lifetime parameters (shown in parentheses) represent the standard error of the mean. [d] The χ_R^2 for a one-exponential fit to the data is shown in parentheses for comparison purposes. Experimental conditions: 25 mM HEPES (or 25 mM HOMOPIPES at pH 5.0), 0.1 M KCl, and either 0.1 mM $CaCl_2$ (+Ca^{2+}) or 0.1 mM EDTA (–Ca^{2+}) at 25 °C. [e] Average amplitudes (α_i) and lifetimes (τ_i) obtained from two-exponential fits to frequency domain data collected for native CaM (λ_{ex} = 275 nm). Uncertainties in measured lifetime parameters (shown in parentheses) are determined from a global error analysis of the parameters, as described in Experimental Procedures and represent 1 standard deviation about the mean. [f] The χ_R^2 for a one-exponential fit to the data is shown in parentheses for comparison purposes. Experimental conditions: 25 mM HEPES (or 25 mM HOMOPIPES at pH 5.0), 0.1 M KCl, and either 0.1 mM $CaCl_2$ (+Ca^{2+}) or 0.1 mM EDTA (–Ca^{2+}) at 25 °C.

rescence intensity decay of either PM-CaM or IASA-CaM in the absence and presence of nitrotyrosine (see above). R_0 is given by:

$$R_0 = 9.79 \times 10^{-5}(n^{-4}\kappa^2\phi_d J)^{1/6} \text{ in cm} \quad (4)$$

where n is the refractive index, κ^2 is the orientation factor, J is the spectral overlap integral, and ϕ_d is the quantum yield of the donor in the absence of acceptor. In our experiments, n is estimated to be 1.40 (Fairclough & Cantor, 1978); κ^2 is assumed to be $^2/_3$, which assumes that donor and acceptor chromophores undergo rapid isotropic rotational motion relative to the lifetime of the donor (see below); ϕ_d is determined by numerical integration of the fluorescence emission spectrum of either PM-CaM or IASA-CaM, using quinine sulfate as a standard, which has a quantum yield of 0.70 in 0.1 N H_2SO_4 (Scott et al., 1970); and J is calculated by numerical integration from the spectra of IASA- and PM-CaM and the absorption spectrum of nitrotyrosine CaM, as described previously for other donor–acceptor pairs (Squier et al., 1987). Color effects relating to the wavelength-dependent properties of the photomultiplier were corrected using an algorithm provided by ISS Inc. (Urbana–Champaign). In the presence of saturating calcium (pH 7.5), the quantum yields (ϕ) for PM-CaM, IASA-CaM, and Tyr_{139} in native CaM are 0.175, 0.193, and 0.022, respectively. The latter measurement is consistent with previous estimates obtained using octopus CaM, which also contains a single tyrosine in calcium binding site IV (Kilhoffer et al., 1981). The overlap integral, J, for the two donor–acceptor pairs PM-nitrotyrosine-CaM and IASA-nitrotyrosine-CaM are 2.80×10^{-15} M^{-1} cm^3 and 2.76×10^{-15} M^{-1} cm^3, respectively. These constants were remeasured under the different experimental conditions used in this study and are reflected in the measured values of R_0 (see Table 3).

Table 2: Stern–Volmer Quenching Constants[a]

	pH	K_{SV} (M^{-1})[c]	$\bar{\tau}$ (ns)[d]	k_q (M^{-1} s^{-1})[d]	k_q/k_q(free probe)[e]
			A. PM-CaM		
free probe[b]	7.5	385	3.9	99×10^9	1.0
$+Ca^{2+}$	7.5	182	13.5	14×10^9	0.14
$-Ca^{2+}$	7.5	69	19.2	3.6×10^9	0.036
$+Ca^{2+}$	5.0	116	19.2	6.0×10^9	0.061
$+Ca^{2+}$ in 6 M GnHCl	7.5	163	3.8	42×10^9	0.43[f]
			B. IASA-CaM		
free probe[b]	7.5	605	0.30	20×10^{11}	1.0
$+Ca^{2+}$	7.5	468	0.70	6.7×10^{11}	0.33
$-Ca^{2+}$	7.5	248	0.73	3.4×10^{11}	0.17
$+Ca^{2+}$	5.0	350	0.89	3.9×10^{11}	0.20
			C. Tyr_{139}		
free probe[b]	7.5	3520	1.05	3.3×10^{12}	1.0
$+Ca^{2+}$	7.5	1330	0.51	2.6×10^{12}	0.78
$-Ca^{2+}$	7.5	520	0.87	0.6×10^{12}	0.18
$+Ca^{2+}$	5.0	206	0.62	0.3×10^{12}	0.10

[a] Protein conformational changes are revealed by changes in solvent accessibility of water soluble quenchers to fluorophores associated with CaM. [b] Free probe is PM-Cys (A), IASA-Cys (B), or L-tyrosine (C). [c] K_{sv} is obtained from the Stern–Volmer relationship $F_0/F = 1 + K_{sv}$[TEMPAMINE], where F_0 is the initial fluorescence intensity in the absence of added quenchers. [d] $k_q \equiv K_{sv}/\bar{\tau}$, where $\bar{\tau} \equiv \sum \alpha_i \tau_i$ (see Table 1). [e] The quenching efficiency of the chromophore bound to CaM was normalized to that of the free probe. [f] k_q/k_q(free probe) corrected for the viscosity of 6 M GnHCl (η = 1.624 cP) relative to pure water (η = 0.89 cP) is 0.70. The concentration of fluorescently labeled calmodulin is 1.13 μM. The concentration of native calmodulin is 5.9 μM. The medium buffer contained 25 mM HEPES (or 25 mM HOMOPIPES at pH 5.0), 0.1 M KCl, and either 0.1 mM $CaCl_2$ ($+Ca^{2+}$) or 0.1 mM EDTA ($-Ca^{2+}$). The temperature was 25 °C.

The above analysis assumes a unique donor–acceptor separation in the calculation of molecular distances, and it ignores any conformational heterogeneity associated with the molecular dynamics of CaM. However, the intensity decay associated with the donor in the presence of an acceptor permits one to recover the conformational heterogeneity (or distribution of distances) associated with CaM [Haas et al., 1978; Beechem & Haas, 1989; reviewed by Cheung (1991)]. To minimize the number of parameters, a uniform Gaussian distribution of donor to acceptor distances, $P(r)$, is generally assumed:

$$P(r) = \exp\left[-\frac{1}{2}\left(\frac{r - R_{av}}{\sigma}\right)^2\right] \quad (5)$$

where R_{av} is the average distance and σ is the standard deviation of the distribution. The width of the distribution is reported as the full width at half-maximum (half-width, hw), which is given by hw = 2.354σ. The adequacy of the Gaussian model is assessed through a comparison of the goodness of the fit (i.e., χ_R^2; see below) relative to the fit using the more general multiexponential model which assumes no physical model.

Decays of Fluorescence Anisotropy. Time-resolved anisotropies were measured both from the phase angle difference and from the ratio of the amplitudes of the parallel and perpendicular components of the modulated emission, as previously described (Lakowicz & Gryczynski, 1991; Johnson & Faunt, 1992).

RESULTS

Specificity of Calmodulin Labeling. Critical to the evaluation of the fluorescence data associated with calcium activation of CaM are (i) the specificity of chemical derivatization and (ii) an assurance that the chemical derivatization did not perturb the structure or function of CaM. Therefore we have characterized the site-directed labeling of wheat germ CaM. Using DTNB to titrate the sulfhydryl content of wheat germ CaM we find 0.95 ± 0.05 mol of SH/mol of CaM, in close agreement with the reported unique Cys_{27} (Yoshida et al., 1983). This indicates that essentially no disulfide cross-links are present. Chemical derivatization of Cys_{27} with either IASA or PM (Figure 1) quantitatively blocks subsequent derivatization with DTNB, suggesting that essentially all cysteines have been derivatized. Quantitation of IASA or PM incorporation using their extinction coefficients (see Experimental Procedures) indicates that 0.88 ± 0.06 mol of IASA/mol of CaM and 0.95 ± 0.03 mol of PM/mol of CaM are covalently incorporated. The incorporation of either IASA or PM onto CaM subsequent to labeling with DTNB [fluorophore content determined following the removal of the thio(nitrobenzoate) blocking group] was negligible (i.e., less than 0.06 mol of IASA or 0.04 mol of PM per mole of DTNB-treated CaM), suggesting that there are no significant labeling sites other than the single cysteine (Cys_{27}).

The specificity of labeling was confirmed using reverse phase HPLC to purify the peptides derived either subsequent to an exhaustive tryptic digestion of native CaM or subsequent to chemical derivatization with PM (data not shown). The retention time of only one peptide is modified following PM labeling of CaM, indicating that a single peptide is modified. Subsequent identification of the modified peptide using mass spectroscopy indicates that tryptic peptide T2 is specifically labeled. T2 contains AA_{15}–AA_{38}, which bracket the single cysteine in wheat germ CaM, consistent with the specific labeling of Cys_{27} with PM (Toda et al., 1985).

In order to measure the spatial separation between Cys_{27} and Tyr_{139} using fluorescence resonance energy transfer (FRET) it is necessary to use a pair of chromophores that have overlapping absorption and fluorescence emission spectra (Stryer, 1978; Haas et al., 1978). In our experiments this requirement is met by modification of Tyr_{139} with TNM and of Cys_{27} with either IASA or PM (Figure 2). The extent of nitration was quantitative (i.e., 0.95 ± 0.05 mol of nitrotyrosine/mol of CaM) as judged by the absorbance spectrum of the modified CaM (see Experimental Procedures). There are no structural or functional perturbations subsequent to nitration as judged by the ability of the modified CaM to activate the erythrocyte Ca-ATPase (see below). Furthermore, any nonspecific nitration of other amino acids will not affect our ability to use nitrotyrosine as an acceptor as the absorbance spectrum of Tyr_{139} is uniquely sensitive to modification by TNM in wheat germ CaM (since there are no tryptophans). However, in order to quantitatively assess the specificity of nitration we subjected the TNM-modified PM-CaM to exhaustive tryptic digestion and compared the resulting tryptic map with that previously generated from PM-CaM. We observe the selective disappearance of T11 (AA_{128}–AA_{144}; Toda et al., 1985), which can no longer be chromatographically detected (data not shown). After the nitration reaction the tryptic maps show an additional set of peaks eluting around 27.0 ± 0.5 min which have spectral characteristics analogous to nitrotyrosine. The intensities and retention times of all other fragments remain unaffected, indicating that the unique tyrosine in wheat germ calmodulin is specifically nitrated.

We have used SDS–PAGE to monitor any cross-linking or fragmentation that may result from either the chemical derivatization of CaM or exposure to ultraviolet light (associated with fluorescence measurements; see below). We observe no changes in the mobility of CaM on SDS–PAGE gels as a result of its covalent modification or exposure to high

Table 3: Donor–Acceptor Separation between Chromophores on Opposing Globular Domains of Calmodulin[a]

	pH	E%[b]	R_o (Å)[c]	r_{app} (Å)[d]	R_{av} (Å)[e]	hw (Å)[e]	χ_R^2
				A. PM Donor			
$+Ca^{2+}$	7.5	35.6	20.6	22.7	22.4	11.8	3.5
		(0.6)	(0.1)	(0.2)	(21.8–23.4)	(10.8–14.0)	
$-Ca^{2+}$	7.5	24.0	21.9	26.5	28.3	19.9	4.3
		(0.4)	(0.1)	(0.2)	(27.2–29.0)	(18.8–22.1)	
$+Ca^{2+}$	5.0	20.3	21.9	27.5	≤28	≥41	3.6
		(0.5)	(0.1)	(0.2)	(0.0–28)	(41–100)	
$+Ca^{2+}$ in 6 M GnHCl	7.5	11.4	17.6	24.5	26.0	22.5	2.2
		(0.2)	(0.1)	(0.3)	(25.6–26.3)	(17.9–26.8)	
				B. IASA Donor			
$+Ca^{2+}$	7.5	32.7	20.8	23.4	19.2	12.3	2.4
		(0.6)	(0.1)	(0.2)	(18.5–20.2)	(11.3–13.4)	
$-Ca^{2+}$	7.5	14.4	20.9	28.1	25.6	19.1	2.6
		(0.3)	(0.1)	(0.2)	(24.9–26.5)	(17.8–20.3)	
$+Ca^{2+}$	5.0	18.1	21.7	27.9	≤21	≥39	3.8
		(0.3)	(0.1)	(0.2)	(0–21)	(39–100)	

[a] Distance measurements obtained from fluorescence resonance energy transfer (FRET) measurements between donor chromophores covalently associated with Cys_{27} and nitrotyrosine 139 in wheat germ CaM. [b] The energy-transfer efficiency is obtained from changes in the fluorescence quantum yield of the donor chromophore using either steady-state measurements or average lifetime measurements (see eq 3) and multiplied by 100. [c] The Förster critical distance represents the distance between a given donor–acceptor pair (under a given set of experimental conditions) where the energy-transfer efficiency is 50%. [d] The apparent donor–acceptor separation assumes that the protein exists in a unique conformation. In all cases described above, the standard error of the mean from either six measurements (PM) or three measurements (IASA) is indicated in parentheses. [e] R_{av} and hw are the average donor–acceptor separation and half-width obtained using the Gaussian distribution model (see Experimental Procedures). The distribution analysis involves a global fit to either six (for PM) or three (for IASA) data sets, as described in Experimental Procedures. The uncertainty in the measured parameters is shown in parentheses and represents 1 standard deviation. Experimental conditions: 25 °C in 25 mM HEPES (or 25 mM HOMOPIPES at pH 5.0), 0.1 M KCl, and either 0.1 mM $CaCl_2$ ($+Ca^{2+}$) or 0.1 mM EDTA ($-Ca^{2+}$).

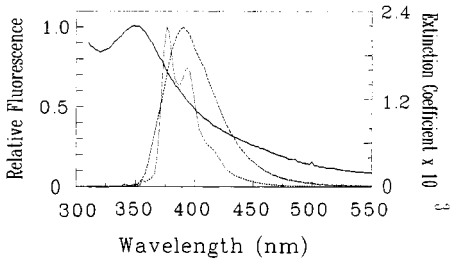

FIGURE 2: Overlap between FRET donor's emission spectrum and absorbance spectrum of acceptor chromophore. Normalized fluorescence emission spectra of *N*-(1-pyrenyl)maleimide-labeled calmodulin (PM-CaM; λ_{ex} = 343 nm; dotted line) and 4-(iodoacetamido)salicylic acid labeled calmodulin (IASA-CaM; λ_{ex} = 302 nm; dashed line) and the absorbance spectrum of nitrotyrosine-calmodulin (solid line). Emission and absorbance spectra were recorded at 1-nm intervals.

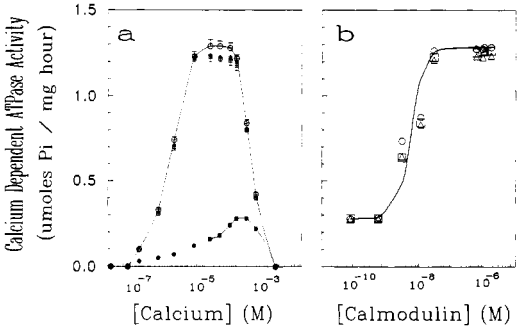

FIGURE 3: Calmodulin stimulation of plasma membrane Ca-ATPase activity. (a) Calcium dependence of Ca^{2+}-dependent ATPase activity of human erythrocyte ghosts in the presence (○, △, □) and absence (●) of CaM. The stimulation of Ca^{2+}-ATPase activity of native CaM (○), PM-nitrotyrosine-CaM (△), and IASA-nitrotyrosine-CaM (□) was compared as a function of free calcium. $CaCl_2$ was added to yield the appropriate free calcium concentration using the metal-binding constants provided by Fabiato and Fabiato (1979) (see Experimental Procedures). In all cases the CaM concentration was 2 μg/mL (0.12 μM). (b) CaM-dependent Ca^{2+}-ATPase activity of the human erythrocyte Ca^{2+}-ATPase was determined at different concentrations of native CaM (○), PM-nitrotyrosine-labeled CaM (△), or IASA-nitrotyrosine-labeled CaM (□). The calculated free calcium concentration was 29.5 μM. In all cases Ca^{2+}-ATPase activity was measured at 25 °C in a reaction medium containing 0.4 mg/mL protein (approximately 30 nM Ca-ATPase), 100 mM KCl, 5 mM $MgCl_2$, 4 μM A23187, 100 μM EDTA, and 25 mM MOPS (pH 7.0).

levels of ultraviolet light (i.e., 6 h; data not shown). Much lower exposure times (less than 1 h) are used for the measurement of the fluorescence data. In all cases CaM migrates as a single major band with an apparent molecular weight of 16.9 kDa.

Biological Activity of Labeled CaM. The utility of these wheat germ CaM derivatives depends on their ability to probe the protein's native structure, which is best assessed by monitoring biological function. IASA-nitrotyrosine-CaM and PM-nitrotyrosine-CaM were compared with native CaM for their abilities to activate the plasma membrane Ca-ATPase of human erythrocyte ghost membranes (Figure 3). This calcium pump contains an autoregulatory domain that binds CaM resulting in both enhanced calcium affinity and enhanced transport activity [reviewed by Carafoli (1992)]. Spectroscopic derivatives of CaM have functional properties nearly identical to those of the native CaM, and they enhance both the calcium affinity (K_d = 0.8 uM) and turnover velocity [V_{max} = 1.2 μmol of P_i/(mg h)] in a manner that is virtually indistinguishable from the native CaM (Figure 3a). Likewise, if we compare the apparent affinity of native and spectroscopic derivatives of CaM for the Ca-ATPase, we find the same activation pattern and apparent K_D for CaM activation of 4 ± 1 nM (Figure 3b). Thus, these spectroscopic derivatives of CaM behave like the native unmodified CaM and can be used to productively examine the structural changes associated with calcium activation of CaM.

Calcium Activation of CaM. Calcium-dependent changes in the fluorescence of native (Tyr_{139}) and PM-labeled (Cys_{27}) CaM were used to assess calcium-dependent structural changes associated with both amino and carboxyl globular domains of CaM (Figure 4). Free calcium concentrations were calculated using the published binding constants to describe the equilibrium between calcium and all added ligands (Fabiato & Fabiato, 1979). Titrations were performed using a range of chelator concentrations (from 0.1 to 2.0 mM EGTA). In all

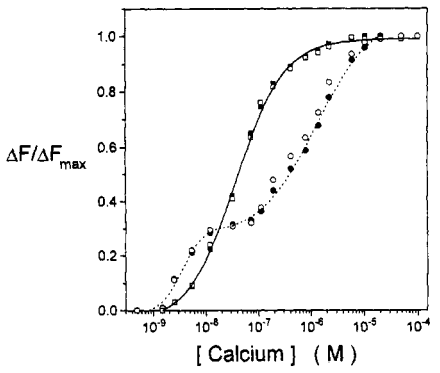

FIGURE 4: Calcium-dependent changes in fluorescence intensity associated with calcium activation of CaM. Calcium-dependent changes in the steady-state fluorescence intensity of both Tyr_{139} (●, ○) and PM-CaM (Cys_{27}; ■, □) were compared as a function of free calcium. Sample conditions included either 3 μM CaM (●, ○) or 0.6 μM CaM (■, □) in 100 mM KCl, 25 mM HEPES (pH 7.5), and either 100 μM EDTA (●, ■) or 200 μM EDTA (○, □). $CaCl_2$ was added to yield the appropriate free calcium concentration (see Experimental Procedures). Maximal changes in the steady-state fluorescence intensity of Tyr_{139} and PM-CaM were +11% and −34%, respectively.

cases the free calcium concentration was checked using the fluorescent calcium indicator FURA-2, and the apparent affinity of calcium for FURA-2 was about 0.1 μM. Independent of the concentration of EGTA (or EDTA; data not shown) used to buffer calcium, we observe a 34% decrease and 11% increase in the fluorescence intensity of PM-CaM (Cys_{27}) and native CaM (Tyr_{139}), respectively, upon increasing the free calcium concentration from 1 nM to 100 μM. However, the use of 2 mM EGTA to buffer the free calcium decreases the apparent calcium affinity of CaM by 1–2 orders of magnitude, suggesting a direct interaction between EGTA and CaM. Therefore, all calcium titrations were carried out at relatively low EGTA (or EDTA) concentrations. The addition of 1 mM $MgCl_2$ results in no change in the steady-state fluorescence signal, indicating that the observed structural changes are specifically associated with calcium binding.

Similar changes are observed in both the steady-state fluorescence and average lifetime of PM-CaM upon calcium binding (Table 1; see below), indicating that the changes in fluorescence associated with calcium binding reflect alterations in the polarity of the fluorophore's environment and provide a reliable indication of a more global structural change surrounding these chromophores (Royer, 1993). However, the 11% increase in the steady-state fluorescence intensity of Tyr_{139} upon calcium binding is associated with a 41% decrease in the average lifetime (Table 1, section C), suggesting that calcium binding to neighboring acidic side chains removes a static component associated with fluorescence quenching [reviewed by Ross et al. (1992)]. Increasing the free calcium concentration to 3.0 mM results in no further change in fluorescence intensity, indicating that no additional structural changes occur in the globular domains surrounding these probes. Therefore, the structural changes associated with calcium activation of CaM are complete under conditions associated with maximal activation of the PM-Ca-ATPase (i.e., ≈5 μM free calcium; Figure 3a). However, when the free calcium concentration exceeds 3 mM, one observes a dramatic increase (decrease) in the steady-state fluorescence intensity of PM-CaM (Tyr_{139}), suggesting that additional structural changes are associated with calcium binding to a population of low-affinity sites.

A systematic variation of the free calcium concentration reveals that changes in the fluorescence intensity of Tyr_{139} are biphasic, suggesting that the Tyr_{139} is sensitive to the binding of two classes of calcium sites ($K_1 \approx 4$ nM, $K_2 \approx 1.1$ μM). Occupancy of the second class of binding sites occurs over the free calcium concentration range associated with activation of the erythrocyte Ca-ATPase (Figure 3a). In contrast, the calcium-dependent changes in the fluorescence intensity of PM-CaM increase monophasically over the same broad range of calcium concentrations associated with activation of the erythrocyte Ca-ATPase ($K_d \approx 40$ nM). These results suggest that the environment around Cys_{27} is sensitive to the occupancy of a single class of calcium-binding sites, probably associated with the amino terminus of CaM. The biphasic sensitivity of Tyr_{139} to calcium binding suggests an ordered binding mechanism, consistent with previous suggestions that calcium occupancy of calcium binding sites III and IV in the carboxyl domain precedes binding to calcium binding sites I and II in the amino-terminal domain [Ikura et al., 1983; Hennessey et al., 1987; reviewed by Williams (1992)]. Therefore, it is reasonable to assign the first class of calcium-binding sites ($K_1 \approx 4$ nm) sensed by Tyr_{139} to be associated with the carboxyl domain, and the second class of calcium-binding sites ($K_2 \approx$ 1.1 μM) sensed by Tyr_{139} to be associated with the amino-terminal domain of CaM. These results suggest long-range structural coupling associated with the occupancy of all four high-affinity calcium-binding sites, that involve either direct interactions between globular domains associated with calcium binding or an allosteric transition associated with the central helix. Likewise, at pH 5.0 (conditions analogous to those used to obtain the crystal structure of CaM) we also observe calcium-dependent changes in both the steady-state fluorescence and lifetime of these chromophores, suggesting that similar structural changes occur upon calcium binding, albeit with a reduced calcium affinity (data now shown). However, at pH 5.0 the calcium-dependent changes in fluorescence are incomplete at 0.1 mM Ca^{2+}, consistent with the decreased affinity of the calcium-binding sites at acidic pH.

Measurement of Fluorescence Lifetime Data. We have measured the fluorescence decay of PM-CaM and IASA-CaM under a range of conditions in order to probe both possible differences in the structure of CaM (i) at pH 7.5 relative to pH 5.0 and (ii) as a function of calcium activation. Utilizing frequency domain fluorescence spectroscopy to measure the lifetime of PM-CaM, we measured the phase lag and demodulation of intensity-modulated light at 23 frequencies between 0.4 and 110 MHz (data not shown). The intensity decay of PM-CaM can be adequately described as a sum of three exponentials, as evidenced by the residuals that are randomly distributed about the origin. We observe a 60-fold improvement in the goodness of fit (i.e., χ_R^2) for a model involving three exponentials relative to the two-exponential model (Table 1, section A), indicating that this model is statistically justifiable. Inclusion of additional fitting parameters results in no further improvement in χ_R^2.

Changes in the fluorescence lifetime reveal structural changes in the immediate environment of fluorophores. There is a large decrease in the average lifetime of PM-CaM in the presence of calcium at *pH 7.5 relative to pH 5.0*, suggesting that PM (covalently bound to Cys_{27}) is in a more polar environment under physiological conditions (Lakowicz, 1983). One observes a similar pH-dependent change in the lifetime of both IASA (covalently bound to Cys_{27}) and Tyr_{139} (Table 1). This suggests that at neutral pH both globular domains adopt a more open conformation than at pH 5.0, resulting in an increased exposure of these probes to the aqueous solvent (see below). However, the juxtaposition of fluorophores next to polar or charged groups in the interior of a protein results in similar decreases in the lifetime of these fluorophores.

Therefore, additional measurements relating to ligand-dependent changes in the environment of these fluorophores are necessary to unambiguously interpret these spectroscopic changes in terms of protein structural changes (see below).

Likewise, *upon calcium binding at pH 7.5* the observed decrease in average fluorescence lifetime of either PM-CaM or Tyr_{139} (Table 1) suggests that these reporter groups in calcium binding loops I and IV become more solvent accessible. In contrast, we observe only a small decrease in the fluorescence lifetime of the more polar IASA label upon calcium binding (Table 1, section B), suggesting that the polar environment surrounding the IASA label does not dramatically change upon calcium binding at physiological pH. Therefore, even though both PM and IASA covalently label Cys_{27}, these probes are located in very different environments. This is consistent with the observed kinetics of labeling, which indicates that PM rapidly labels Cys_{27} in the native conformation, while it is necessary to first denature CaM to gain access to Cys_{27} by IASA (see Experimental Procedures). This suggests that Cys_{27} is buried in the protein matrix, and that the more hydrophobic PM gains access to this site at a significant rate while the more polar IASA chromophore is excluded.

Ca^{2+}-Induced Changes in Probe Accessibility. In order to explicitly define the solvent accessibility of the probe sites, we measured the accessibility of both PM and IASA (covalently bound to Cys_{27}) and Tyr_{139} to water soluble quenchers of fluorescence (i.e., KI and the spin label TEMPAMINE). The latter quencher has the advantage of greater quenching efficiency, allowing its use at low concentrations without significantly altering the ionic strength. A comparison of the solvent accessibility of calcium-saturated CaM to TEMPAMINE at pH 7.5 relative to pH 5.0 to external quenchers indicates 2- and 8-fold increases in the accessibility of PM (or IASA; both covalently bound to Cys_{27}) and Tyr_{139}, respectively (Table 2), consistent with the observed decrease in the average lifetime (see above). Similar changes in solvent accessibility are observed using KI (data not shown), suggesting that changes in the quenching efficiency are a result of changes in solvent accessibility and are not affected by any specific (e.g., electrostatic) interactions between CaM and the quencher. This indicates that both the amino and carboxyl globular domains associated with these chromophores adopt a more open structure at physiological pH. Likewise, a comparison of changes in solvent accessibility of all three fluorophores associated with calcium binding at pH 7.5 indicates that there is a 2–4-fold increase in solvent accessibility (Table 2). This indicates that both the amino and carboxyl globular domains adopt a more open tertiary conformation upon calcium binding.

Spatial Separation between Globular Domains. Utilizing FRET we were able to measure the apparent distance (r_{app}) between chromophores covalently linked to Cys_{27} (i.e., PM and IASA) and nitrotyrosine 139. This involves the calculation of r_{app} between chromophores using either the relative steady-state fluorescence or the average lifetime of the donor in the presence and absence of acceptor (Table 1; eq 3). These complementary measurements yield nearly identical energy-transfer efficiencies, indicating that there is no static component in the measured energy-transfer efficiency. This agreement suggests that there is no significant population of donor–acceptor probes located within $0.5R_0$ for either donor–acceptor pair (Lakowicz, 1983). For all subsequent analysis regarding the spatial separation between donor–acceptor chromophores we have emphasized the use of the lifetime measurements. This involves the measurement of the phase lag and modulation of PM-CaM or IASA-CaM (data not shown) in the presence and absence of the acceptor, nitrotyrosine. One observes in all cases that the frequency response is shifted to higher frequencies in the presence of acceptor, indicating that the average lifetime becomes shorter.

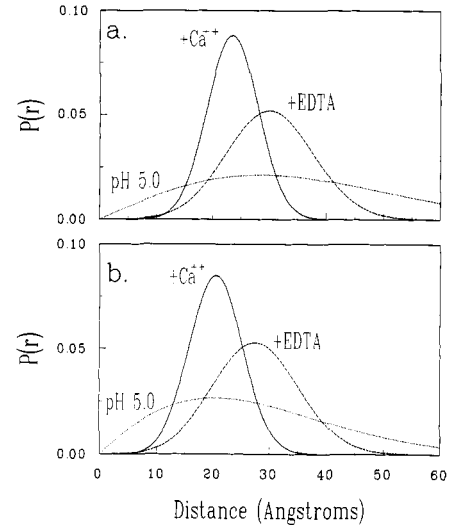

FIGURE 5: Distance distribution for the separation between Cys_{27} and Tyr_{139} in CaM. Depiction of the uniform Gaussian distribution of distances calculated between donor (PM, a; or IASA, b) and acceptor chromophores (nitrotyrosine 139; a and b) calculated from a global fit to six to eight data sets. Sample conditions: 1.13 μM CaM, 0.1 M KCl, 25 mM HEPES (pH 7.5; solid or dashed lines) or 25 mM HOMOPIPES (pH 5.0; dotted line) in the presence of either 0.1 mM $CaCl_2$ (solid and dotted lines) or 0.1 mM EDTA (dashed line). The sample temperature was 25 °C.

We observe significant changes in energy-transfer efficiency both as a function of pH and upon calcium binding (Table 3). Upon calcium binding at pH 7.5 the energy-transfer efficiency increases by 11.6% ± 0.7% and 18.3% ± 0.7% for PM-nitrotyrosine-CaM and IASA-nitrotyrosine-CaM, respectively. These results suggest that upon calcium binding the apparent separation between chromophores placed at Cys_{27} and Tyr_{139} becomes 4–5 Å closer. In contrast, if one compares the average separation between these chromophores at pH 5.0 ($+Ca^{2+}$) relative to pH 7.5 ($+Ca^{2+}$), one finds a 4–5-Å increase in the apparent distance between these donor and acceptor probes, such that the average separation between these probes is now 27–28 Å (Table 3). This distance closely resembles the separation between these analogous side chains in the crystal structure of CaM (Babu et al., 1988).

Distance Distribution Analysis of FRET Data. The frequency domain intensity decays of PM-CaM and IASA-CaM in the presence and absence of nitrotyrosine were used to recover the time-dependent terms relating to the distribution of distances between these two donor–acceptor pairs (Table 3). This model explicitly considers the conformational heterogeneity of macromolecules (Haas et al., 1978; Lakowicz et al., 1988; Beechem & Haas, 1989). We find that the average donor–acceptor distance (R_{av}) recovered from the distance distribution model is analogous to the results obtained using averaged lifetimes (i.e., r_{app}; Table 3). Upon calcium binding at pH 7.5 we observe a 6-Å decrease in the average donor–acceptor distance, independent of the donor–acceptor pair.

However, we find that the half-width of the distance distribution becomes much narrower upon calcium binding (i.e., 11–12 Å) relative to the half-width in the presence of EDTA (i.e., 19–20 Å; Table 3 and Figure 5), suggesting that the central helix becomes more rigid. There is a systematic 2–3-Å difference in the recovered distance distribution for PM-nitrotyrosine-CaM and IASA-nitrotyrosine-CaM, consistent with the previously discussed differences in the

conformation of these covalently bound probes (see above). A rigorous error analysis of the recovered distance distribution of both donor–acceptor pairs (see above) was used to assess the certainty of the recovered distribution. This analysis assesses for the cross-correlation between calculated parameters (i.e., R_{av} and half-width; Beechem et al., 1991). The parameter of interest is systematically altered, and all other parameters are varied so as to minimize the normalized χ_R^2 (i.e., χ_N^2). A determination of the experimental uncertainty involves an assessment of the increase in χ_N^2 associated with a defined probability (i.e., a horizontal line is drawn at 67% probability; Bevington, 1969) that the measured parameter is contained within the error surface. The error surfaces are relatively narrow for both donor–acceptor pairs (Table 3), emphasizing the statistically significant change in both R_{av} and half-width associated with calcium binding at pH 7.5. The fact that the recovered half-widths are virtually the same suggests that the contribution of independent probe motion to the recovered distribution is relatively minor.

In contrast, when the data collected at pH 5.0 ($+Ca^{2+}$) is fitted to the distance distribution model we obtain a very broad distance distribution using both donor–acceptor pairs (Figure 5 and Table 3). However, while the distribution model is able to adequately fit the data (as judged by the χ_R^2), an analysis of the error surfaces (i.e., χ_R^2) of the recovered average donor–acceptor separation (R_{av}) and half-width is poorly defined at pH 5.0 (Table 3). While we do not currently understand the underlying physical reason for the large uncertainty in the recovered distance distribution at pH 5.0, it is nevertheless clear that the distribution of distances between both donors located at Cys_{27} and nitrotyrosine 139 is very broad (i.e., half-width $\geq$ 39 Å). This indicates that there is considerable conformational heterogeneity with respect to the spatial relationship between the two globular domains at pH 5.0.

The additional information provided by the distance distribution model can be further appreciated by the observation that, upon denaturation, there is little change in the apparent separation (r_{app}) between the PM-nitrotyrosine donor–acceptor pair on CaM (Table 3). However, using the distance distribution model one observes a significant increase in the conformational heterogeneity associated with CaM under denaturing conditions (i.e., the half-width for the distance distribution increases from 11.8 Å to 22.5 Å in the presence of 6.0 M GnHCl; Table 3), consistent with the expected disruption of CaM's tertiary structure upon exposure to chaotropic agents. Analogous results have been reported for troponin I (Lakowicz et al., 1988), emphasizing the need to utilize realistic models to appreciate ligand-dependent changes in the spatial separation between donor–acceptor chromophores.

Rotational Dynamics of CaM. In order to define dynamic conformational changes associated with calcium binding we have used frequency domain measurements of fluorescence anisotropy of both PM-CaM and native CAM (i.e., Tyr_{139}). These measurements permit us to assess both (i) segmental mobility and (ii) the overall motion of CaM. While segmental mobility provides information relating to the environment around the chromophore and is thus complementary to our previous lifetime and quenching measurements, the global rotational motion of CaM is sensitive to the overall dimensions of the protein. PM has a relatively long lifetime, permitting measurements of the overall rotational motion of CaM. Complementary measurements of the rotational dynamics of Tyr_{139} were undertaken in order to assess the environmental changes in the carboxyl domain of CaM upon calcium activation as well as to better define the errors associated with

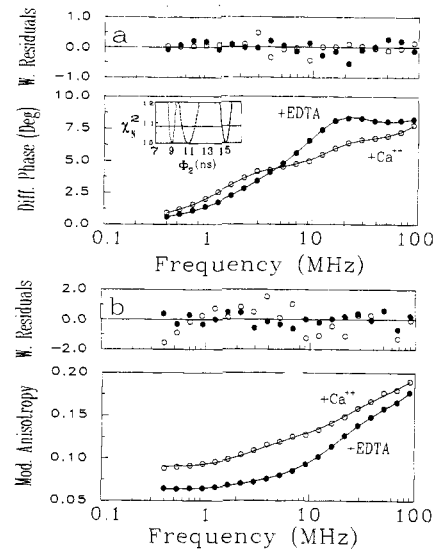

FIGURE 6: Frequency domain anisotropy data for PM-CaM. Data are shown for +Ca (○) and +EDTA (●) for the differential phase (a) and modulated anisotropy (b). The assumed errors for the phase and modulation are 0.2° and 0.005, respectively. The medium buffer contained 1.13 μM PM-CaM, 0.1 M KCl, and either 0.1 mM $CaCl_2$ or 0.1 mM EDTA added to the buffer (25 mM HEPES at pH 7.5 or 25 mM HOMOPIPES at pH 5.0). The temperature was 25 °C. Inset: Dependence of normalized chi squared (χ_N^2) on the rotational correlation time of PM-CaM. Dashed line: +Ca, pH 7.5. Dotted line: +EDTA, pH 7.5. Solid line: +Ca, pH 5.0.

the measurement of distances using nitrotyrosine 139 as an energy-transfer acceptor (see below).

We collected data over 20 frequencies between 0.4 and 90 MHz (Figure 6). Upon increasing the frequency we observe that both the differential phase (Figure 6a) and modulation anisotropy (Figure 6b) progressively increase. Using algorithms previously described (Weber, 1981), we find that a sum of two exponentials is required to adequately describe the data, as judged by both the 40–50-fold reduction in χ_R^2 and the evenly distributed residuals (Figure 6). Inclusion of additional fitting parameters results in no significant improvement in the calculated fit to the data.

Segmental Rotational Dynamics. Upon calcium binding (pH 7.5) we observe a significant change in the measured differential phase and modulation anisotropy (Figure 6). The amplitude (i.e., $g_1 r_0$) and rate ($1/\phi_1$) of rotational motion associated with the segmental motion of PM both increase upon calcium binding (Table 4), consistent with earlier measurements that indicate that the globular domains adopt a more open tertiary structure upon calcium binding (see above). Upon denaturation of CaM in 6 M GnHCl we observe a further increase in the rotational dynamics of PM, consistent with the local unfolding of the globular domains. Likewise we observe a small increase in rotational dynamics upon raising the pH from 5.0 to 7.5, consistent with a more exposed environment around PM at pH 7.5. Similar changes in the rotational dynamics of Tyr_{139} are observed upon either calcium binding or changing the pH, consistent with our previous suggestions (see above) that upon calcium binding (or increasing the pH from 5.0 to 7.5) both globular domains adopt a more open structure.

Overall Rotational Dynamics of CaM. While the energy-transfer measurements already discussed indicate that the conformational heterogeneity associated with the central helix is dramatically reduced upon calcium binding at pH 7.5 (see above), the calcium-dependent changes in the conformation of the globular domains do not allow one to unambiguously interpret the data in terms relating to the nature of the calcium-

Table 4: Rotational Dynamics of PM-CaM and Tyr_{139} Calmodulin[a]

	pH	P[b]	g_1r_0[c]	ϕ_1 (ns)[d]	g_2r_0[c]	ϕ_2 (ns)[d]	χ_R^2[e]
			A. PM-Cys_{27}CaM				
$+Ca^{2+}$	7.5	0.078	0.16	0.8	0.11	10.9	0.50
			(0.01)	(0.1)	(0.01)	(0.7)	(20.4)
$-Ca^{2+}$	7.5	0.059	0.13	1.4	0.11	8.8	0.20
			(0.01)	(0.1)	(0.01)	(0.3)	(11.8)
$+Ca^{2+}$	5.0	0.091	0.14	1.0	0.11	15.2	0.21
			(0.01)	(0.1)	(0.01)	(0.4)	(10.1)
$+Ca^{2+}$ in 6 M GnHCl	7.5	0.12	0.20	0.56	0.075	17.7[f]	0.52
			(0.01)	(0.05)	(0.07)	(1.3)	(24.4)
			B. Tyr_{139}CaM				
$+Ca^{2+}$	7.5	0.29	0.18	0.5	0.15	⟨10.9⟩[g]	0.71
			(0.01)	(0.1)	(0.01)		(25.9)
$-Ca^{2+}$	7.5	0.29	0.16	0.8	0.17	⟨8.8⟩[g]	0.86
			(0.01)	(0.1)	(0.01)		(2.3)
$+Ca^{2+}$	5.0	0.28	0.16	0.6	0.17	⟨15.2⟩[g]	1.4
			(0.01)	(0.1)	(0.01)		(3.2)

[a] Steady-state and time-resolved measurements of the rotational dynamics of either PM (A) or tyrosine (B) were used to assess ligand- or pH-dependent changes in either the segmental or overall rotational dynamics of CaM. The time-resolved data are obtained from a multiexponential fit. [b] P is the steady-state polarization, where $P \equiv (I_\parallel - gI_\perp)/(I_\parallel + gI_\perp)$. $I_\parallel$ and $I_\perp$ refer to the steady-state fluorescence intensity obtained using vertically polarized light as an excitation source when the emission polarizer is in the vertical and horizontal directions, respectively. The g factor corrects for imperfections in the polarizers, where upon excitation with horizontally polarized light $g \equiv I_\parallel/I_\perp$. [c] g_ir_0 are the amplitudes of the total anisotropy associated with each rotational correlation time (ϕ_i). [d] ϕ_1 and ϕ_2 are the rotational correlation times associated with segmental and overall protein rotational motion. [e] χ_R^2 describes the deviations between the model and experimental data (see Experimental Procedures). The number in parentheses represents the χ_R^2 obtained for a one-component fit to the data. [f] ϕ_2 corrected for the viscosity of 6 M GnHCl (η = 1.624 cP) relative to pure water (η = 0.89 cP) is 9.7 ns. [g] ϕ_2 was fixed with respect to global rotational motion of CaM as determined using PM-CaM. Buffer contained 25 mM HEPES (or 25 mM HOMOPIPES at pH 5.0), 0.1 M KCl, and either 0.1 mM $CaCl_2$ ($+Ca^{2+}$) or 0.1 mM EDTA ($-Ca^{2+}$). The temperature was 25 °C.

dependent change in the average conformation of the central helix (i.e., does the central helix become more extended, or is a bent conformation favored). Using the PM fluorophore, we were able to directly measure the hydrodynamic properties of CaM, permitting us to assess the overall dimensions of CaM [reviewed by Steiner (1991)]. For comparison purposes the expected rotational correlation time for an equivalent hydrated globular protein of molecular weight 16 900 Da whose partial specific volume is 0.707 cm^3/g (Crouch & Klee, 1980) is 7.0 ns, where

$$\phi_2 = \frac{\eta V}{kT}$$

η is the viscosity of water (i.e., 0.89 cP at 25 °C), V is the hydrated volume of CaM (i.e., 3.24×10^4 Å^3 assuming two water shells of hydration; Cantor & Schimmel, 1980), k is Boltzmann's constant, and T is the absolute temperature (i.e., 298 K). We find that the correlation time associated with the rotational mobility along CaM's principle axis changes from 8.8 ± 0.3 ns to 10.9 ± 0.7 ns upon calcium binding at pH 7.5 (Table 4), indicating (i) that CaM is a nonspherical molecule and (ii) that CaM becomes more extended upon calcium binding. This suggests that the decreased conformational heterogeneity associated with the central helix (see above) corresponds to a more elongated central helix. Assuming that the structure of CaM is analogous to that observed in the crystal structure, the calcium-dependent increase in the correlation time corresponds to a 5–8-Å increase in the principle axis of CaM (Small & Anderson, 1988). A rigorous analysis of the errors associated with the measurement of CaM's rotational dynamics was assessed to account for all correlations between the measured parameters. In this analysis, the correlation time (i.e., ϕ_2) is systematically varied, and all other parameters are varied to optimize the fit to the data (i.e., minimize χ_N^2, where χ_R^2 has been normalized; see Experimental Procedures). A horizontal line is drawn corresponding to the increase in χ_N^2 that corresponds to 1 standard deviation (Bevington, 1969). The increase in correlation time upon calcium binding is statistically significant, as judged by the nonoverlapping error surfaces (Figure 6, inset).

In order to directly relate the observed correlation times to the crystal structure, we measured CaM's rotational dynamics under analogous conditions (i.e., pH 5.0). Under these acidic conditions the correlation time of CaM increases substantially relative to that observed at pH 7.5 (from 10.9 ± 0.7 ns to 15.2 ± 0.4 ns), and suggests that (i) the rotational dynamics of both globular domains remain tightly coupled through the central helix and (ii) the overall dimensions of CaM increase by about 5 Å (Small & Anderson, 1988), analogous to the increase in the apparent donor–acceptor separation (Table 3). The observed correlation time at pH 5.0 is similar to that predicted from hydrodynamic models relating to dumbbell-shaped proteins (i.e., $1/6D_\perp$ = 14.7 ns; Garcia de la Torre & Bloomfield, 1981), in which the dimensions obtained from the crystal structure are used as a reference (Babu et al., 1988). This suggests that the average structure adopted by CaM at pH 5.0 is consistent with the crystal structure. However, at pH 5.0 the distance distribution between chromophores located in opposing globular domains becomes conformationally disordered (Figure 5 and Table 3). Since the globular domains adopt more compact structures at pH 5.0, it is reasonable to associate the increased conformational disorder with the central helix. Analogous distance distributions were obtained using chromophores with very different lifetimes (Figure 5), suggesting that the conformational dynamics associated with the central helix is slow relative to the nanosecond time scale. This is consistent with the increased correlation time observed at pH 5.0, which also indicates that the dynamics associated with the interconversion between conformational substates is slow relative to the time scale of protein rotation.

Upon the addition of 6 M GnHCl to CaM we observe an increase in both the amplitude and rate of segmental motion, consistent with an unfolding of CaM's tertiary structure. The apparent increase in the long correlation time associated with global rotational motion arises from the increased viscosity of the GnHCl. The corrected correlation time represents a modest increase in rotational dynamics (i.e., ϕ_2 = 9.7 ns relative to 10.9 ns for native CaM; Table 4, section A). Under these conditions the globular domains undergo unfolding as measured by both the 5-fold increase in the accessibility of PM to external quenchers (Table 2, section A) and the greater rotational mobility of PM (Table 4, section A). The lack of an appreciable effect of denaturing conditions on the global rotational dynamics of CaM may indicate that elements of calmodulin's secondary and tertiary structure are retained even in the presence of 6 M GnHCl, such that the rotational dynamics of the two opposing globular domains remain coupled.

Evaluation of the Energy-Transfer Orientation Factor (κ^2). As is typical when using FRET to measure molecular distances, we have assumed the orientation between donor and acceptor chromophores to be motionally averaged in the preceding discussion (i.e., κ^2 is taken to be equal to $^2/_3$). However, it is widely recognized that the major uncertainty associated with the calculation of molecular distances from FRET data is the evaluation of the contribution that restrictions in the rotational dynamics of the donor and acceptor chromophores

have on the transfer efficiency [Haas et al., 1978; Dale et al., 1979; reviewed by Cheung (1991)]. Only if the chromophores undergo fast Brownian rotation relative to the lifetime of the donor chromophore is the orientation factor, κ^2, fully averaged (i.e., $\kappa^2 = {}^2/_3$). Various suggestions have been proposed to deal with the problem of the orientational factor in cases where the donor and acceptor do not span all orientations in space during the donor lifetime. The use of different donor–acceptor pairs permits the sampling of different orientational combinations for the donor and acceptor (Stryer & Haugland, 1967), which provides increased confidence in the interpretation of changes in the energy-transfer efficiency in terms of distances. Therefore, in the above measurements we have used two complementary chromophores covalently bound to Cys_{27} that function as energy-transfer donors. These chromophores (i.e., PM and IASA; see Figure 1) have very different physical properties (i.e., covalent linkages, polar character, average excited-state lifetime, and size), and while both probes bind to Cys_{27}, their chromophores associate with different molecular environments (see Table 2). However, in both cases an evaluation of the time-dependent terms associated with energy transfer yield similar distance distributions (Table 3). This provides strong evidence in support of the calculated distance distributions shown in Figure 5.

An alternative and complementary approach aimed at estimating the uncertainty in donor–acceptor separation has been to measure the partial rotational diffusion of the chromophores (as revealed by their fluorescence polarization) to set limits on the range of κ^2 (Dale & Eisinger, 1976; Haas et al., 1978). The errors associated with the estimation of κ^2 can be obtained from the measured rotational dynamics of both the extrinsic probes that serve as energy-transfer donors (i.e., PM and IASA covalently bound at Cys_{27}) and the intrinsic Tyr_{139} that when nitrated serves as an energy-transfer acceptor. In this analysis we assume that the nitration of Tyr_{139} does not significantly change its rotational dynamics. In the case of the FRET donors we find that these probes undergo fast reorientation relative to the time scale of FRET as indicated both by the low steady-state polarization (i.e., $P < 0.1$ for both PM and IASA), and by the larger relative amplitude associated with the nanosecond rotational dynamics of these probes (Table 4; data not shown for IASA). Likewise, Tyr_{139} undergoes rapid rotational motion relative to the time scale of the FRET measurement (Table 4), although the significant steady-state polarization (i.e., $P \approx 0.29$ under all ligand conditions) indicates that the rotational mobility of Tyr_{139} is restricted during its subnanosecond excited-state lifetime (Table 2). The assumption of a single transition moment associated with both donor and acceptor chromophores permits a conservative estimation of the errors associated with the calculation of R_0 (Dale et al., 1979; Cheung, 1991). Assuming the fundamental anisotropy (r_f) to be 0.4 for both donor and acceptor, the calculated range of κ^2 for the PM–nitrotyrosine donor–acceptor pair varies from 0.29 to 2.05 ($+Ca^{2+}$, pH 7.5), resulting in variations in r_{app} of 3–4 Å. This analysis, however, ignores the mixed polarization of both donor and acceptor chromophores (Haas et al., 1978), which acts to further reduce the probable errors associated with the measured distance separation. Tabulated values of the effects of the orientation of donor and acceptor chromophores (as determined from steady-state polarization values) on the calculation of distances from the energy-transfer data indicate a probable error of no more then 7% (i.e., 1–2 Å) associated with the calculation of the molecular distances between Cys_{27} and nitrotyrosine 139 (Haas et al., 1978). Analogous errors in the measured distances are observed for the other conditions (i.e., +EDTA or pH 5.0). It is therefore concluded that the assumption that $\kappa^2 = {}^2/_3$ does not dramatically affect the nature of the recovered distance distribution associated with protein conformational heterogeneity.

DISCUSSION

An understanding of the changes in both the dynamics and average structure of CaM upon calcium activation is critical to a mechanistic appreciation of calcium regulation in cellular metabolism. It is currently clear that calcium binding is associated with the exposure of hydrophobic binding sites [reviewed by Strynadka and James (1991)], which allow both the amino and carboxyl globular domains to bind conserved amphipathic target sequences [reviewed by Ikura et al. (1992a)]. Detailed models have been proposed to account for the structural changes in CaM's globular domains coincident with calcium binding, which suggest that calcium binding involves a large reorientation of the helices by up to 14 Å (Strynadka & James, 1988). These models are based upon the homology between the globular domains in CaM and troponin C, whose crystal structure contains calcium bound only to the carboxyl domain (Herzberg et al., 1986). In the latter case, the structural differences between the two domans in troponin C are taken as indicative of the structural changes that result from calcium binding. These models do not take into account structural differences between the globular domains and the central helix in the crystal structure relative to that observed in solution (Trewhella et al., 1989; Török et al., 1992; Wang, 1989; Barbato et al., 1992). Therefore, direct measurements relating to both the local and global structural changes associated with calcium binding to CaM under physiological conditions are needed.

Our approach involves the use of site-directed fluorescence probes located in calcium binding sites I and IV, which permit the identification of calcium-dependent changes associated with the conformation and dynamics of both the central helix and globular domains. Lifetime-resolved FRET measurements detect both the average separation and distance heterogeneity between fluorophores associated with the opposing domains within CaM and provide a direct measure of conformational heterogeneity of the central helix. Complementary measurements regarding the local environment of fluorophores located within the globular domains (i.e., dynamic quenching and rotational dynamics) as well as the global rotational dynamics provide a consistent interpretation regarding the structural changes associated with the activation of CaM (see below).

Summary of Results. Lifetime-resolved FRET measurements between donor and acceptor chromophores placed within the opposing globular domains within CaM indicate that upon calcium binding there is a large decrease in both the average and distance and conformational heterogeneity between Cys_{27} and Tyr_{139} (Figure 5, Table 3). This is consistent with two disparate models that involve either (i) a bent central helix that brings the opposing globular domains into close proximity or (ii) an elongated central helix, which would require structural changes associated with the globular domains that compensate for the reduced range of conformations available to the central helix. To differentiate between these models we measured both the accessibility and dynamics of fluorophores associated with both globular domains in CaM, permitting us to assess localized structural changes associated with each globular domain. Upon calcium binding we find a 2–3-fold increase in both the solvent accessibility and rotational dynamics of fluorophores located by Cys_{27} and Tyr_{139} (Table 2), indicating that both globular domains adopt

more open conformations. There is a corresponding decrease in the average lifetime (Table 1), consistent with an increased polarity surrounding these fluorophores (Lakowicz, 1983). Likewise, the labeling kinetics of both Cys_{27} and Tyr_{139} are enhanced upon calcium binding, consistent with a model in which both the amino and carboxyl domains adopt more open tertiary structures subsequent to calcium activation.

The rotational dynamics associated with overall protein tumbling decreases upon calcium binding (Table 4), indicating that the principle axis of CaM becomes elongated. Therefore, calcium activation of CaM corresponds to (i) a generalized structural change (involving a more open conformation) associated with both globular domains such that the average distance between Cys_{27} and Tyr_{139} is decreased 4–6 Å with (ii) a large reduction of the conformational flexibility associated with the central helix, such that the half-width of the distance distribution is reduced by 7–8 Å (Table 3). The more open conformation assumed by the globular domains may enhance the conformational heterogeneity associated with the distance between the two chromophores associated with calcium binding sites I and IV, and therefore the change in the half-width of the distribution is probably an underestimation of the structural changes associated with the central helix upon calcium binding. The exposure of the peptide binding sites in the globular domains with the concomitant decrease in conformational heterogeneity is proposed to be essential to the rapid association of CaM with target sequences.

In order to obtain information regarding the relationship between the solution structure under physiological conditions and that observed in the crystal structure, we have contrasted the structural properties of CaM at pH 7.5 relative to pH 5.0, which approximate the conditions used to obtain the crystal structure. At pH 5.0 the globular domains of CaM adopt a more compact structure in comparison to the calcium-bound structure at pH 7.5, as indicated by both the increased lifetime and 2-fold reduction in the solvent accessibility of either Tyr_{139} or covalent fluorophores bound to Cys_{27} (Tables 1 and 2). In comparison, both decreases in the efficiency of FRET between the chromophores at Cys_{27} and nitrotyrosine 139 and decreases in the rotational dynamics associated with overall protein rotational motion indicate a more elongated structure at acidic pH (Tables 3 and 4), which is associated with a large increase in the conformational heterogeneity of the central helix. The increased conformational heterogeneity may be associated with the high density of acidic amino acids located in the central helix (i.e., Asp_{78}, Asp_{80}, Glu_{82}, Glu_{83}, Glu_{84}, and Glu_{87}; Babu et al., 1988), which would be expected to have anomalously high pK_a's and therefore may be protonated when the pH of the bulk solvent is near pH 5.0. This would remove constraints associated with the conformational freedom of the purported flexible linker region in the central helix (Asp_{78}–Ser_{81}; Ikura et al., 1991) and is consistent with the structural roles played by Asp_{78} and Glu_{82} in stabilizing the central helix in the crystal structure (Chattopadhyaya et al., 1992). Likewise, the replacement of glutamic acid side chains in this linker region using site-directed mutagenesis alters the ability of CaM to activate some target proteins (Craig et al., 1987), suggesting a critical role for these amino acids in facilitating the correct association with the target enzyme. In this regard it should be remembered that the central helix is predicted to be relatively unstable [reviewed by Kretsinger (1992a,b)]. These results suggest an important role for the deprotonated acidic residues located within the central helix in limiting protein conformational flexibility.

Relationship to Other Studies: Local Structural Changes. Numerous previous studies involving both chemical derivatization, changes in the affinity of hydrophobic drugs, and spectroscopic changes associated with either the local environment or secondary structure of CaM have detected structural changes associated with calcium binding that expose hydrophobic binding sites for target proteins (Walsh & Stevens, 1977; LaPorte et al., 1981; Thiry et al., 1980; Johnson & Wittenauer, 1983; Tanaka et al., 1983; Burger et al., 1984; Krebs et al., 1984; Jarret, 1984; Zimmer & Hoffman, 1987; Guerini et al., 1987; Gryczynski et al., 19088; Gryczynski et al., 1991). Far-UV circular dichroism, optical rotary dispersion, and FT-IR measurements all suggest that calcium binding is associated with a small increase in α-helical content (Liu & Cheung, 1976; Burger et al., 1984; Hennessey et al., 1987; Trewhella et al., 1989), although the latter measurements indicate that a substantial fraction of the α-helical content in the calcium-saturated form of CaM arises from a distorted α-helix that contains additional hydrogen bonding to water [reviewed by Trewhella (1992)]. Given the small change in partial specific volume associated with calcium binding (i.e., 0.712 cm^3/g to 0.707 cm^3/g) (Crouch & Klee, 1980), it is reasonable to suppose that the distorted α-helical region may be associated with the exposed central helix and may alter the spatial disposition of the two globular domains in a manner that may facilitate their interaction with target peptides. In addition, the calcium-dependent change in α-helical content may account for the calcium-dependent increase in the overall dimensions of CaM (Seaton et al., 1985; Heidorn & Trewhella, 1988; Small & Anderson, 1988; this work). Previous time-resolved fluorescence measurements relating to the structure of the globular domains in CaM have likewise detected decreases in the rotational dynamics associated with the two tyrosine residues present in calcium binding loops III and IV from bovine calmodulin [Bayley et al., 1988; Gryczynski et al., 1988; Gryczynski et al., 1991; Török et al., 1992; reviewed by Anderson (1991)]. While the spatial arrangement of these two tyrosines does not appreciably change upon calcium binding (Steiner & Montevalli-Alibadi, 1984; Steiner et al., 1991), any change in their relative orientation or rotational dynamics upon calcium binding would greatly affect the documented resonance energy transfer between these tyrosines (Gryczynski et al., 1988). Therefore, it is not possible to make a molecular interpretation regarding the calcium-dependent change in rotational dynamics associated with the two tyrosines in animal CaM. Nevertheless, these results are consistent with the proposal that calcium binding acts to rigidify CaM's structure [reviewed by Williams (1992)].

Relationship to Other Studies: Global Structural Changes. The possibility that the opposing globular domains in CaM are allosterically coupled through the central helix was suggested as a result of the fact that calcium binding sites II and III are shared with the central helix in the crystal structure (Babu et al., 1985, 1988). However, little evidence has been provided to support a direct role for structural changes associated with the central helix in the calcium activation of CaM. Subsequent to the modification of either the length or composition of the central helix, CaM retains its ability to activate target proteins (Persechini & Kretsinger, 1988a). Furthermore, substitution of the central helix with a synthetic linker (i.e., bismaleimidohexane between cysteines engineered at amino acid positions 3 and 146) retains the ability of CaM to fully activate some (but not all) target proteins (Persechini & Kretsinger, 1988a,b). These results are consistent with the observation that the central helix in the calcium-saturated form of CaM has been found to be highly flexible, permitting both globular domains to specifically associate with target proteins subsequent to calcium activation. These results

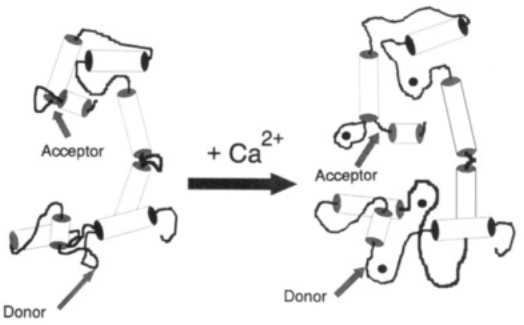

FIGURE 7: Model illustrating the conformational changes coincident with calcium activation of calmodulin: illustration that calcium binding is associated with (i) the adoption of a more open structure associated with the globular domains; (ii) an increased proximity between donor (D) and acceptor (A) chromophores associated with Cys_{27} and Tyr_{139}, respectively; and (iii) an elongated central helix that becomes more rigid. Cylinders represent α-helices, lines represent calcium-binding loops or disordered structure, and filled circles represent calcium ligands. The line separating the two cylinders near the center of the central helix represents a flexible loop, as described previously (Ikura et al., 1992a,b). The model does not attempt to depict detailed structural features present in the high-resolution structure obtained using X-ray diffraction. However, the globular domains in the cartoon are purposely depicted in a more open conformation relative to that observed in the crystal structure, as discussed in the text.

suggest that the central helix may play a nonspecific role, serving as a "flexible tether" that functions to keep the two globular domains of CaM in close proximity for subsequent binding to target sequences, and are consistent with previous suggestions (based on the analogous physical properties between the proteolytic fragments containing either globular domain and the intact protein) that both globular domains in CaM bind calcium independently of one another (Dalgarno et al., 1984; Ikura et al., 1985; Martin et al., 1985; Drakenberg et al., 1987). However, these experiments do not address changes in the conformational heterogeneity and dynamics of the central helix (measured in this study), which may play an important role in facilitating the rate of binding to target proteins, which is critical to CaM's ability to regulate cellular metabolism in response to rapidly changing levels of cellular calcium. Our results suggest a structural coupling between the opposing globular domains in CaM, consistent with earlier optical and NMR measurements regarding the hydrodynamic properties of CaM, which likewise indicate a structural coupling between the opposing globular domains through the central helix (Small & Anderson, 1988; Török et al., 1992). However, this interpretation remains controversial (Barbato et al., 1992).

Model for Calcium Activation of CaM. We have presented evidence that upon calcium binding (i) Cys_{27} and Tyr_{139} become more accessible to solvent (Table 2) and experience greater segmental rotational motion (Table 4), (ii) the distance and conformational heterogeneity between Cys_{27} and Tyr_{139} is reduced (Figure 5, Table 3), and (iii) CaM becomes more elongated (Tables 3 and 4). This suggests that (a) the globular domains of CaM become more open, permitting the easy access of solvent to the chromophore and bringing the donor–acceptor pair into closer proximity, and (b) the central helix becomes more rigid, resulting in reduced conformational heterogeneity and in an elongated molecule with an increased rotational correlation time. A model depicting the average conformational changes associated with calcium binding is summarized in Figure 7. The underlying mechanism for this conformational change involves correlated structural changes of both the globular domains and the central helix, consistent with earlier suggestions of a possible coupling between the central helix (which comprises a portion of calcium binding sites II and III) and the opposing globular domains in CaM (Babu et al., 1988).

ACKNOWLEDGMENT

We wish to thank David Johnson, Gale Strasburg, and Diana Bigelow for their encouragement and many helpful discussions. We wish to thank the Center for Fluorescence Spectroscopy (Baltimore, MD) for making their software available.

REFERENCES

Anderson, S. R. (1991) *J. Biol. Chem. 266*, 11405–11408.
Babu, Y. S., Sack, J. S., Greenough, T. J., Bugg, C. E., Means, A. R., & Cook, W. J. (1985) *Nature 315*, 37–40.
Babu, Y. S., Bugg, C. E., & Cook, W. J. (1988) *J. Mol. Biol. 204*, 191–204.
Barbato, G., Ikura, M., Kay, L. E., Pastor, R. W., & Bax, A. (1992) *Biochemistry 31*, 5269–5278.
Bayley, P., Martin, S., & Jones, G. (1988) *FEBS Lett. 238*, 61–66.
Bayley, P. M., & Martin, S. R. (1992) *Biochim. Biophys. Acta 1160*, 16–21.
Beechem, J. M., & Haas, E. (1989) *Biophys. J. 55*, 1225–1236.
Beechem, J. M., Gratton, E., Ameloot, M., Knutson, J. R., & Brand, L. (1991) in *Topics in Fluorescence Spectroscopy* (Lakowicz, J. R., Ed.) pp 241–305, Plenum Press, New York.
Bevington, P. R. (1969) *Data Reduction and Error Analysis for the Physical Sciences*, McGraw-Hill, New York.
Burger, D., Cox, J. A., Comte, M., & Stein, E. A. (1984) *Biochemistry 23*, 1966–1971.
Cantor, C. R., & Schimmel, P. R. (1980) *Biophysical Chemistry*, Vol. 2, W. H. Freeman and Company, San Francisco.
Carafoli, E. (1992) *J. Biol. Chem. 267*, 2115–2118.
Chattopadhyaya, R., Meador, W. E., Means, A. R., & Quicho, F. A. (1992) *J. Mol. Biol. 228*, 1177–1192.
Cheung, H. C. (1991) in *Topics in Fluorescence Spectroscopy* (Lakowicz, J. R., Ed.) Vol. 2, pp 128–176, Plenum Press, New York.
Cheung, W. Y. (1980) *Science 207*, 19–27.
Craig, T. A., Watterson, D. M., Prendergast, F. G., Haiech, J., & Roberts, D. M. (1987) *J. Biol. Chem. 262*, 3278–3284.
Crouch, T. H., & Klee, C. B. (1980) *Biochemistry 19*, 3692–3698.
Dale, R. E., & Eisinger, J. (1976) *Proc. Natl. Acad. Sci. U.S.A. 73*, 271–273.
Dale, R. E., Eisinger, J., & Blumberg, W. E. (1979) *Biophys. J. 26*, 161–194.
Dalgarno, D. C., Klevit, R. E., Levine, B. A., Williams, R. J. P., Dobrowolski, Z., & Drabikowki, W. (1984) *Eur. J. Biochem. 138*, 281–289.
Drabikowski, F. (1987 *Calcium transport in contraction and secretion* (Margreth, W. A., Ed.) pp 469–478, North Holland Publishing, Amsterdam.
Drakenberg, T., Forsen, S., Thulin, E., & Vogel, H. J. (1987) *J. Biol. Chem. 262*, 672–678.
Ellman, G. L. (1959) *Arch. Biochem. Biophys. 82*, 70–77.
Fabiato, A. (1988) *Methods Enzymol. 157*, 378–417.
Fabiato, A., & Fabiato, F. (1979) *J. Physiol. (Paris) 75*, 463–505.
Fairclough, R. H., & Cantor, C. R. (1978) *Methods Enzymol. 48*, 347–379.
Garcia de la Torre, J., & Bloomfield, V. (1981) *Q. Rev. Biophys. 14*, 81–139.
Gratton, E., & Limkeman, M. (1983) *Biophys. J. 44*, 315–324.
Gryczynski, I., Lakowicz, J. R., & Steiner, R. F. (1988) *Biophys. Chem. 30*, 49–59.
Gryczynski, I., Steiner, R. F., & Lakowicz, J. R. (1991) *Biophys. Chem. 39*, 69–78.
Guerini, D., Krebs, J., & Carafoli, E. (1987) *Eur. J. Biochem. 170*, 35–42.

Haas, E., Katchalski-Katzir, E., & Steinberg, I. (1978) *Biochemistry 17*, 5064–5070.
Haugland, R. P. (1992) *Handbook of Fluorescent Probes and Research Chemicals*, 5th ed., Molecular Probes, Inc., Eugene, OR.
Heidorn, D. B., & Trewhella, J. (1988) *Biochemistry 27*, 909–915.
Hennessey, J. P., Manavalan, P., Johnson, W. C., Malencik, D. A., Anderson, S. R., Schimerlik, M. I., Shalitin, Y. (1987) *Biopolymers 26*, 561–571.
Herzberg, O., Moult, J., & James, M. N. G. (1986) *J. Biol. Chem. 261*, 2638–2644.
Ikura, M., Hiraoki, M., Mikuni, T., Yazawa, M., & Yagi, K. (1983) *Biochemistry 22*, 2573–2579.
Ikura, M., Minowa, O., & Hikichi, K. (1985) *Biochemistry 24*, 4264–4269.
Ikura, M., Kays, L. E., Krinks, M., & Bax, A. (1991) *Biochemistry 30*, 5498–5504.
Ikura, M., Barbato, G., & Bax, A. (1992a) *Cell Calcium 13*, 391–400.
Ikura, M., Clore, G. M., Gronenborn, A. M., Zhu, G., Klee, C. B., & Bax, A. (1992b) *Science 256*, 632–638.
Jarret, H. W. (1984) *J. Biol. Chem. 259*, 10136–10144.
Johnson, J. D. (1983) *Biochem. Biophys. Res. Commun. 112*, 787–793.
Johnson, J. D., & Wittenauer, L. A. (1983) *Biochem. J. 211*, 473–479.
Johnson, M. L., & Faunt, L. M. (1992) *Methods Enzymol. 210*, 1–37.
Kataoka, M., Head, J. F., Seaton, B. A., & Engelman, D. M. (1989) *Proc. Natl. Acad. Sci. U.S.A. 86*, 6944–6948.
Kilhoffer, M. C., Demaille, J. G., & Gérard, D. (1981) *Biochemistry 20*, 4407–4414.
Klee, C. (1988) in *Calmodulin* (Cohen, P., & Klee, C. B., Eds.) pp 35–56, Elsevier, New York.
Klee, C. B., Crouch, T. H., & Richman, P. G. (1980) *Annu. Rev. Biochem. 49*, 489–515.
Krebs, J., Buerkler, J., Guerini, D., Brunner, J., & Carafoli, E. (1984) *Biochemistry 23*, 400–403.
Kretsinger, R. H. (1992a) *Cell Calcium 13*, 363–376.
Kretsinger, R. H. (1992b) *Science 258*, 50–51.
Kretsinger, R. H., & Nockolds, C. E. (1973) *J. Biol. Chem. 248*, 3313–3326.
Lakowicz, J. R. (1983) *Principles of Fluorescence Spectroscopy*, Plenum Publishing Corp., New York.
Lakowicz, J. R., Gryczynski, I. (1991) in *Topics in Fluorescence Spectroscopy* (Lakowicz, J. R., Ed.) Vol. I, pp 293–335, Plenum Press, New York.
Lakowicz, J. R., & Gryczynski, I., Cheung, H. C., Wang, C., Johnson, M. L., & Joshi, N. (1988) *Biochemistry 27*, 9149–9160.
Lanzetta, P. A., Alverez, L. J., Reinsch, P. S., & Candia, O. (1979) *Anal. Biochem. 100*, 95–97.
LaPorte, D. C., Keller, C. H., Olwin, B. B., & Storm, D. R. (1981) *Biochemistry 20*, 3965–3972.
Lehrer, S. S., & Leavis, P. C. (1978) *Methods Enzymol. 49*, 222–236.
Liu, Y. M., & Cheung, W. Y. (1976) *J. Biol. Chem. 251*, 4193–4198.
Luedtke, R., Owen, C. S., Vanderkooi, J. M., & Karush, F. (1981) *Biochemistry 20*, 2927–2936.
Malencik, D. A., & Anderson, S. R. (1987) *Biochemistry 26*, 695–704.
Martin, S. R., Teleman, A., Bayley, P. M., Drakenberg, T., & Forsen, S. (1985) *Eur. J. Biochem. 151*, 543–550.
Matsushima, N., Izumi, Y., Masuo, T., Yoshino, Y., Ueki, T., & Miyake, Y. (1989) *J. Biochem. (Tokyo) 105*, 883–887.
Meador, W. E., Means, A. R., & Quiocho, F. A. (1992) *Science 257*, 1251–1254.
Meador, W. E., Means, A. R., & Quiocho, F. A. (1993) *Science 262*, 1718–1721.
Niggli, V., Penniston, J. T., & Carofoli, E. (1979) *J. Biol. Chem. 254*, 9955–9958.
O'Neil, K. T., & DeGrado, W. F. (1990) *Trends Biochem. Sci. 15*, 59–63.
Persechini, A., & Kretsinger, R. H. (1988a) *J. Biol. Chem. 263*, 12175–12178.
Persechini, A., & Kretsinger, R. H. (1988b) *J. Cardiovasc. Pharmacol. 12*, 1–12.
Richman, P. G., & Klee, C. B. (1978) *Biochemistry 17*, 928–935.
Riordan, J. F., & Vallee, B. L. (1972) *Methods Enzymol. 25B*, 515–521.
Ross, J. B. A., Laws, W. R., Rousslang, K. W., & Wyssbrod, H. R. (1992) in *Topics in Fluorescence Spectroscopy* (Lakowicz, J. R., Ed.) Vol. 3, pp 1–63, Plenum Press, New York.
Royer, C. A. (1993) *Biophys. J. 65*, 9–10.
Scott, T. G., Spencer, R. D., Leonard, N. G., & Weber, G. (1970) *J. Am. Chem. Soc. 92*, 687–695.
Seaton, B. A., Head, J. F., Engelman, D. M., & Richards, F. M. (1985) *Biochemistry 24*, 6740–6743.
Small, E. W., & Anderson, S. R. (1988) *Biochemistry 27*, 419–428.
Squier, T. C., & Thomas, D. D. (1988) *J. Biol. Chem. 263*, 9171–9177.
Squier, T. C., Bigelow, D. J., Garcia de Ancos, J., & Inesi, G. (1987) *J. Biol. Chem. 262*, 4748–4754.
Steiner, R. F. (1991) in *Topics in Fluorescence Spectroscopy* (Lakowicz, J. R., Ed.) Vol. 2, pp 1–52, Plenum Press, New York.
Steiner, R. F., & Montevalli-Alibadi, M. (1984) *Arch. Biochem. Biophys. 234*, 522–530.
Steiner, R. F., Albaugh, S., Kilhoffer, M.-C. (1991) *J. Fluoresc. 1*, 15–22.
Strasburg, G. M., Hogan, M., Birmachu, W., Thomas, D. D., & Louis, C. F. (1988) *J. Biol. Chem. 263*, 542–548.
Stryer, L. (1978) *Annu. Rev. Biochem. 47*, 819–846.
Stryer, L., & Haugland, R. P. (1967) *Proc. Natl. Acad. Sci. U.S.A. 58*, 719–726.
Strynadka, N. C. J., & James, M. N. G. (1988) *Proteins 3*, 1–17.
Strynadka, N. C. J., & James, M. N. G. (1991) *Curr. Opin. Struct. Biol. 1*, 905–914.
Tanaka, T., & Hidaka, H. (1980) *J. Biol. Chem. 255*, 1078–1080.
Tanaka, T., Ohmura, T., & Hidaka, H. (1983) *Pharmacology 26*, 249–257.
Thiry, P., Van Dermeers, A., Van Dermeers-Piret, M. C., Rathe, J., & Chrisotpe, J. (1980) *Eur. J. Biochem. 103*, 409–414.
Thulin, E., Andersson, A., Drakenberg, T., Forsen, S., & Vogel, H. J. (1984) *Biochemistry 23*, 1862–1870.
Toda, H., Yazawa, M., Sakiyama, F., & Yagi, K. (1985) *J. Biochem. 98*, 833–842.
Török, K., Lane, A. N., Martin, S. R., Janot, J.-M., & Bayley, P. M. (1992) *Biochemistry 31*, 3452–3462.
Trewhella, J. (1992) *Cell Calcium 13*, 377–390.
Trewhella, J., Liddle, W. K., Heidorn, D. B., & Strynadka, N. (1989) *Biochemistry 28*, 1294–1300.
Walsh, M., & Stevens, F. C. (1977) *Biochemistry 16*, 2742–2749.
Wang, C.-L. A. (1989) *Biochemistry 28*, 4816–4820.
Weber, G. (1981) *J. Phys. Chem. 85*, 949–953.
Williams, R. J. P. (1992) *Cell Calcium 13*, 355–362.
Wylie, D. C., & Vanaman, T. C. (1988) in *Calmodulin* (Cohen, P., & Klee, C. B., Eds.) pp 1–16, Elsevier, New York.
Yazawa, M., Vorherr, P., James, P., Carafoli, E., & Yagi, K. (1992) *Biochemistry 31*, 3171–3176.
Yoshida, M., Minowa, O., & Yagi, K. (1983) *J. Biochem. (Tokyo) 94*, 1925–1933.
Zimmer, M., & Hoffman, F. (1987) *Eur. J. Biochem. 164*, 411–420.